Seismic Efficiency during Volcanic Unrest: Insights from the 2010 Eyjafjallajökull Eruption

Authors: James Dalziel[1,2], Juliet Biggs[2], Heidy Mader[2], Max Werner[2]

[1]Willis Research Network, Willis Group Limited, 51 Lime Street, London, UK, EC3M 7DQ. Email: james.dalziel@wtwco.com ORCiD: 0000-0002-0341-3260

[2]School of Earth Sciences, University of Bristol, Bristol, UK, BS8 1RJ.

Abstract:

Identifying patterns in precursory signals may aid forecasting over month to year timescales. Here we examine the relationship between seismicity and ground deformation during unrest prior to the 2010 Eyjafjallajökull eruption. We find that the ratio between seismic moment and horizontal GPS ground displacement is constant within two distinct phases, but with a step increase from one to the other. This step-change is attributed to a change in source between two sills, and is expected given the change in deformation associated with different source geometries and deformation mechanisms. We use displacement data to estimate source volume change, assuming each source has a fixed geometry through time. We can then calculate seismic efficiency (the ratio between seismic moment and volume change, assuming a constant shear modulus). An increase in seismic efficiency is also present between sources, indicating different growth mechanisms. The shallower source has a lower proportion of aseismic deformation, consistent with previous observations showing clusters of seismic events, interpreted as a number of magmatic 'lobes' separated by seismogenic zones. This case study provides new insights into subsurface processes prior to eruptive activity, specifically controls on the seismic efficiency of intrusions.

1. Introduction:

The monitoring of volcanic systems has greatly improved over the past few decades, with techniques such as real-time seismic monitoring using broad-band seismometers and satellite observations of ground deformation to provide continuous and high-quality datasets (Sparks 2003, Vila et al. 2008, Sparks et al. 2012). Despite this, there is still difficulty differentiating between deformation sources, notably between magmatic, tectonic and hydrothermal activity (Sandri et al. 2004, Battaglia et al. 2008, Pritchard et al. 2019). The processes causing these different forms of activity can determine whether or not an unrest episode will lead to eruption (Lopez et al. 2017), and so accurate and timely interpretation of these signals are important in order to offer suitable advice as part of the forecasting process (Illsley-Kemp et al. 2021).

The characterisation of individual monitoring datasets, such as the number of earthquakes or seismic energy release during unrest, to help forecast the timing or strength of an eruption (Cornelius & Voight 1995, Sandri et al. 2004). Analysis of different streams of monitoring data against one another is less explored, and the opportunity to examine changes in relationship between these datasets may yield new insights into the precursory processes occurring within volcanic systems (e.g. Reath et al. 2020). Multiparameter studies can be conducted using laboratory experiments (Kilburn 2012), in analogue environments such as wastewater injection into wells (McGarr 2014), during precursory unrest prior to volcanic eruptions (White & McCausland 2016, Meyer et al. 2021), and at volcanoes with repeated or cyclic activity (Bell et al. 2021).

Here we focus on geophysical proxies for stress and strain, specifically seismicity and deformation. Previous comparisons between seismic moment and volume change have looked at total values prior

to eruption (White & McCausland 2016, Meyer et al. 2021), and here we aim to examine the relationship over time, and relate it to the processes that occur during an unrest episode (e.g. Schmid et al. 2012, Sheldrake et al. 2017, Bell et al. 2021).

Testing the relationship between deformation and seismicity through time using volcano monitoring data can give an insight into the geometry and characteristics of sub-surface magma sources. Here we use the concept of seismic efficiency, $S_{EFF} = \frac{\Sigma M_0}{G\Delta V}$ where M_0 is the seismic moment and ΔV is the total volume of injected fluid (Hallo et al. 2014). G is the shear modulus which can be estimated based on depth (e.g. Heap et al. 2020).

Seismic efficiency has been widely used for studying induced seismicity, where it is used to analyse seismicity rates against fluid injection rates to calibrate site-specific pore pressure models for more accurate hazard forecasting and mitigation strategies (Verdon et al. 2024). We apply the concept of seismic efficiency to a volcano case study for the first time, using the example of coupled volcano-tectonic earthquakes and ground deformation prior to the 2010 Eyjafjallajökull eruption in Iceland. We expect that depth and temperature will be the primary control on whether deformation occurs elastically (high seismic efficiency) or viscoelasticly (low seismic efficiency). We examine our results against both shear modulus and seismic efficiency, in order to determine the mechanism driving the change in relationship between seismicity and source volume change.

2. Background:

The disposal of wastewater from hydraulic fracturing for oil and gas extraction by injection into deep aquifers shows a power-law relationship between seismic moment and volume of injected wells (McGarr 2014). White & McCausland (2016) found a similar relationship for volcanoes, based on the analysis of X periods of unrest and proposed that total intruded volume and therefore eruption size can be estimated based on the seismicity observed during precursory unrest. Reanalysis of geodetically studied seismic swarms during volcanic unrest also found a power-law relationship however with higher volume change relative to moment and more spread (Meyer et al. 2021).

Time-series analysis of synthetic and real-world seismicity data show that the rate of earthquake occurrence and seismic energy release increase exponentially in the days before eruption (Bell et al. 2011, Bell et al. 2013). A similar trend is also seen in the total number of earthquakes and event magnitudes over inter-event periods at Sierra Negra from 2004 to 2020 (Bell et al. 2021). However, this is not always the case. For example, seismic unrest prior to the 2017 – 2019 eruption at Mt. Agung, Bali peaked in late September and slowed before the eruption onset in late November (Syahbana et al. 2019). This period of decreased seismic activity complicated forecasting efforts, and showed that more complex volcano-tectonic interactions can occur at some volcanic settings (Albino et al. 2019, Wellik et al. 2021).

Ground deformation shows more complex evolution (Biggs & Pritchard 2017). Studies examining time series deformation from volcanic sources reveals different signals, with both longer-term steady-state and shorter-term pulsatory inflation noted for African volcanoes (Biggs et al. 2011, Albino et al. 2022), and episodic magma injection into interconnected magmatic systems causing correlations in uplift and subsidence for neighbouring volcanoes in the Galapagos (Reddin et al. 2023). For case study volcanoes in Indonesia, periods of inflation were found to preclude eruptions in some but not all cases (Chaussard & Amelung 2012), depending on the pressure state of the magmatic plumbing system beforehand.

2.1 Case Study Volcanoes

Table 1. Seismicity vs. deformation relationships		
Paper	**Case Studies**	**Relationship**
Bell et al. 2021	Time series moment vs. uplift during unrest at Sierra Negra, 2012 – 2018	Power law
McGarr 2014	Total moment vs. volume at 18 fluid injection sites for hydraulic fracturing, wastewater disposal into deep aquifers & geothermal system development	Power law
Meyer et al. 2021	Total moment vs. intruded volume for unrest prior to 17 volcanic eruptions	Power law
Schmid et al. 2012	Time series cumulative seismic events vs. displacement at Piton de la Fournaise between 22 eruptions, 1999 – 2006	Exponential seismicity, linear displacement

An example of time-series data used in analysis of the number of earthquakes and seismic moment against vertical uplift at Sierra Negra volcano (Bell et al. 2021) reveals an exponential increase in seismicity relative to uplift prior to the 2018 eruption. Both the number of events and moment show a power-law relationship with uplift. This time-series relationship appears similar to studies of moment and volume change such as McGarr (2014) and Meyer et al. (2021), and although Sierra Negra monitoring data only considers vertical deformation, magma accumulation within a shallow sill makes this likely the most representative aspect of ground movement. If the magmatic complex contained multiple sources of differing geometries, inclusion of horizontal deformation or modelling of intruded volume change may be necessary for accurate comparison against seismic moment and analysis of the relationship between them. Variations within the overall power-law relationship produced from Bell et al.'s (2021) data appear promising, as these may reflect changes in subsurface processes that could be characterised and used to help identify if unrest may lead to eruption and constrain when this may occur.

At Piton de la Fournaise, Schmid et al. (2012) show exponential increases in earthquake rate prior to all eruptions, with cumulative displacement showing more diverse behaviour. Over periods of several months between events, a sequence of exponential increases followed by exponential decreases in displacement rate is present. This trend in displacement is also seen at Laguna del Maule between 2003 and 2014 (Le Mével et al. 2015). In the days immediately preceding eruptions the rate of displacement shows a consistent increase, but with both linear and exponential trends seen over varying timescales. When the data for 22 eruption events are stacked to observe overall trends, seismicity shows an exponential increase from approximately 700 to 1400 events/day over 25 days prior to onset, whereas displacement shows a slower linear increase of approximately 0.2mm/day over 100 days before eruption. This example suggests that a single volcano undergoing repeated episodes of unrest exhibit patterns in precursory monitoring data, which could make forecasting of future episodes more robust if enough historic data are present.

2.2 Eyjafjallajökull 2010 Case Study:

We select a case study eruption with well-studied and comprehensive monitoring data available, in order to test the relationship between deformation and seismic moment. The unrest episode chosen was prior to the 2010 Eyjafjallajökull eruption, due to the monitoring data and literature available (e.g. Sigmundsson et al. 2010, Tarasewicz et al. 2012, 2014, Keiding & Sigmarsson 2012, Meinsopust et al. 2014). Monitoring data presented by Sigmundsson et al. (2010) comprised radial vector (relative to Eyjafjallajökull's summit) horizontal ground displacement from GPS, hereafter referred to as 'radial

displacement', intruded volume changes calculated from inverse modelling of InSAR, number of seismic events with a minimum local magnitude (M_L) of completeness of ≥0.8, seismic moment (assumed to be calculated from local magnitude via scaling equations, although this is not stated), magma compositions from the two phases of eruption, and timescales for different phases of activity for the period 1st September 2009 to 28th April 2010. An approximate source geometry for the pre-eruptive complex was determined by Sigmundsson et al. (2010) to comprise two sills at different depths ('Sill 1' and 'Sill 2'), both fed from a deeper source, and a 'Tilted Dyke' (hereafter referred to as 'Dyke') connecting both sills to ground surface at the location of effusive flank eruption (Figure 1).

Intermittent unrest episodes preceding the 2010 eruption had been ongoing since 1991, when seismicity increased after over twenty years of quiescence (Sigmundsson et al. 2010). Periods of ground displacement that occurred alongside earthquake swarms modelled using GPS and InSAR determined that two sills were emplaced in 1994 and 1999, at depths of 4.5km and 6.3km respectively (Pederson & Sigmundsson 2004, 2006). Seismicity in 1996 also indicated the emplacement of a deep intrusion near the base of the crust at a depth of 20-25km (Hjaltadóttir et al. 2009, Tarasewicz et al. 2014), correlating with evidence of a deflating deep source during the 2010 eruption episode.

Prior to the 2010 eruption, unrest began with a swarm of 200 earthquakes occurring between June – August 2009, located north-east of the summit crater at a depth of 9-11km (Hjaltadóttir et al. 2009). The seismicity was accompanied by 10-12mm of southward ground movement, recorded by GPS station 'THEY' (seen in Figure 1a). This activity likely related to the onset of magma movement from the deep intrusion towards the shallower crust. The rate of seismicity and ground deformation then again increased substantially from January 2010 until the onset of the effusive flank eruption, and is the period of unrest studied for this project. In early March daily radial displacement is stated to consistently increase to >5mm/day (Sigmundsson et al. 2010). A spike in seismicity is also shown from this date, though this is not commented on by Sigmundsson et al. (2010).

Detailed study of seismicity in the two weeks prior to flank eruption was conducted using three-dimensional mapping of earthquake hypocentres (Tarasewicz et al. 2012, 2014), agreeing that seismicity was caused by a complex of laterally inflating sills at ~4-5km depth and an eastward-propagating dyke that rose to ~2-3km depth four days prior to eruption, reaching ground surface on 20th March 2010. Far-field GPS measurements also indicated that inflation of the sills was fed by magma from a deflating deep source at >20km depth (Hreinsdóttir et al. 2012, Tarasewicz et al. 2012). Figure 1a and 1b show plan and section views of the area studied, overlain with eruption locations, monitoring stations used to collect data, and source outlines determined from joint inversion of GPS and InSAR data.

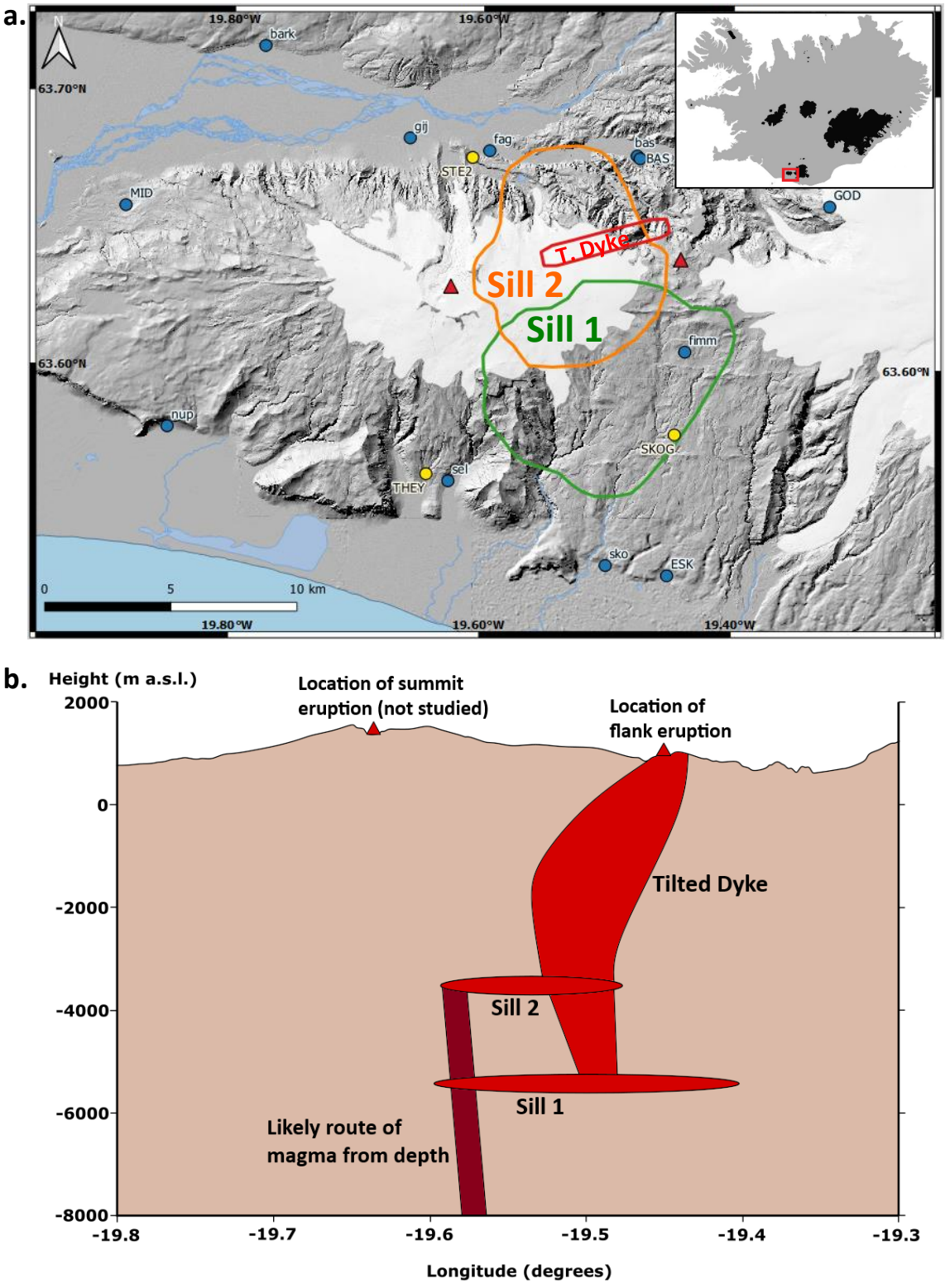

Figure 1: Plan and cross-section views of Eyjafjallajökull case study area. a. Plan view topography, hydrology, and glaciers, overlain with GPS stations (yellow) and seismometers (blue) used to obtain monitoring data. Red triangles show locations of effusive flank (R) and explosive summit (L) eruptions. Outlines show approx. source extent from InSAR for Sill 1 (green), Sill 2 (orange) and the Dyke (red), adapted from Sigmundsson et al. (2010). Inset shows location of study area (red) and prominent glaciers (black). b. Cartoon cross-section of magmatic complex, based on available seismic foci from Tarasewicz et al. (2014) and information from Sigmundsson et al. (2010). Sources from unrest episodes in 1994 and 1999, as well as associated with explosive summit eruption not shown.

Monitoring data presented within Sigmundsson et al. (2010) comprised seismic moment, number of earthquake events and radial displacement data. From these data, we plotted displacement and seismicity against time to identify any anomalous results, noise or gaps.

Table 2: Sigmundsson et al. (2010) source parameter ranges

	Dates	Depth	Radius	Volume
Sill 1	01/01/2010 – 04/03/2010	4.0 – 5.9km	3.1 – 5.0km	$0.9 – 1.6\times10^7$ m^3
Sill 2	05/03/2010 – 20/03/2010	3.9 – 6.0km	2.7 – 3.3km	$1.5 – 2.7\times10^7$ m^3
Dyke	05/03/2010 – 20/03/2010*	2.0 – 5.6km (lower edge), 10s – 100s m (upper edge)	-	$1.9 – 4.8\times10^7$ m^3

* Sigmundsson et al.'s (2010) analysis suggested that Sill 2 and the Dyke intruded simultaneously.

Sigmundsson et al. (2010) analysed source volume change from inversion of InSAR and GPS displacement data, with assessment of potential error resulting in a range of total volume changes for each proposed source. The averages for these volume change ranges were 1.2×10^7 m^3 for Sill 1, 1.8×10^7 m^3 for Sill 2, and 3.0×10^7 m^3 for the Dyke, with the sills modelled as penny-shaped cracks (Fialko et al. 2001) and the Dyke as rectangular with a constant opening (Okada 1985). The full range of source parameters presented by Sigmundsson et al. (2010) are detailed in Table 2. However, limitations in the temporal resolution of InSAR imagery may lead to discrepancies when comparing these volume changes against time series GPS data. GPS is therefore the primary form of displacement data considered for this study, with InSAR serving as a means of checking accuracy when modelling source volume change.

Following inspection of monitoring data presented by Sigmundsson et al. (2010), a new study period following the onset of seismicity up until the first effusive fissure eruption was selected for further analysis (31/01/2010 to 20/03/2010). This time period was selected as initial activity beforehand showed large gaps and significant noise for displacement data, and therefore was not thought to be reliable. The period after eruption onset is not needed, as the study was concerned with pre-eruptive unrest. This study period was more accurately split into periods associated with the three magmatic sources (Sill 1: 31/01/2010 to 04/03/2010, Sill 2: 05/03/2010 to 16/03/2010, Dyke: 17/03/2010 to 20/03/2010) after more detailed post-processing of monitoring data undertaken during this study.

The decision was made to start the study period from the 31st January 2010 due to lack of GPS deformation data beforehand, with station 'SKOG' showing gaps throughout December and January and station 'STE2' not commencing until late February. A previous station 'STEI' had been present in the same location as 'STE2', but appeared to be non-operational between October 2009 and February 2010 and so was replaced. Deformation data available prior to the beginning of the study period showed little definitive directional movement that would indicate sill inflation, even after the onset of seismicity. However, it should be noted that if Sill 1 intrusion had begun before the study period, any minor deformation not included could result in modelled source volume changes not being accounted for and thus estimated total source volume change being inaccurate. The end of the study period is easier to clearly define, as the onset of the effusive flank eruption on the 20/03/2010 is well documented in literature and marks the transition from increasing displacement to negligible or decreasing displacement according to the data presented by Sigmundsson et al. (2010).

3. Methods and Results:

3.1 Post-processing GPS ground displacement prior to eruption:

Radial displacement data presented by Sigmundsson et al. (2010) allowed for preliminary analysis of unrest, however the use of vector projection from Eyjafjallajökull's summit meant this data was not an ideal proxy for stress when examining the magmatic complex feeding the fissure eruption. Therefore, processed GPS monitoring data from the IMO was obtained from FutureVolc's 'Two Volcanoes' database (https://blog.vedur.is/twovolcanos/eyja/); comprising east, north and vertical displacement at nine stations around the summit between June 2009 – September 2010. Of these GPS datasets, stations 'THEY' and 'SKOG' located ~9km south-west and ~6km south-east of the centre of the magmatic complex respectively (seen within Figure 1a), provided the best examples of ground movements for analysis of subsurface magma movements prior to eruption. Ground movement recorded by these stations could therefore be plotted to show the direction and intensity of displacement during our study period. A third GPS station 'STE2', located ~7km north-west of the magmatic complex, showed incomplete data with significant gaps until late February 2010, and thereafter provided a comprehensive but relatively unclear record of displacement. This station was therefore discounted early in the study where datasets were analysed individually, but was revisited when data from the three stations was used in source modelling.

Plotting the east and north components of daily GPS movement as an XY scatter plot for THEY and SKOG reveals the direction and intensity of ground displacement during the study period, which can help to determine the location and changes within the magma plumbing system prior to eruption (examples in Figures 2 and 3). Vertical displacement data was also studied for evidence of changes, but was not deemed useful at this stage due to a high degree of noise and potential error.

In order to analyse daily displacement across the whole study period, conversion of IMO horizontal displacement data into movement along vectors that most accurately represent the motion associated with each magmatic source was undertaken. Data presented by Sigmundsson et al. (2010) showed the magnitude of radial displacement from Eyjafjallajökull's summit to each GPS station, which was not considered suitable for this study as the magmatic complex was offset to the east of the summit and comprised sources offset from one another. Instead, movement was fitted along different vectors according to changes in the direction of movement associated with each source. This method was achieved by isolating the data for each change in horizontal movement direction from a single GPS station and plotting it as a scatter graph with north-south and east-west axes, fitting a trendline to each subset, and converting the bearing (θ) of the trend line into a vector (e.g. east; θ = 90°, south; θ = 180°, and so on). An example of this method using data from station 'SKOG' for the proposed Sill 1 is shown in Figure 2.

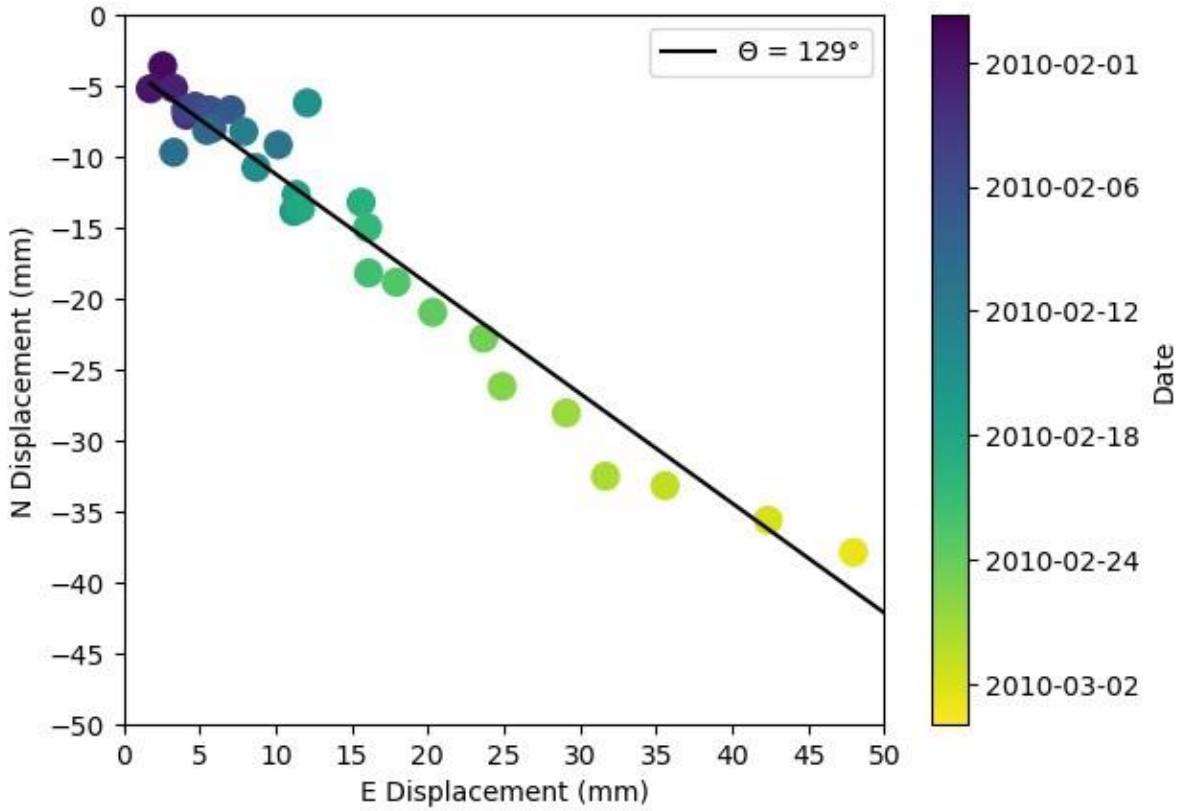

Figure 2: Derivation of 'best fit vector' for GPS station 'SKOG' horizontal displacement data from 31/01/2010 to 04/03/2010 (associated with proposed Sill 1), coloured by date of occurrence. A best fit line is plotted for displacement data during this period, and the angle from the Y-axis is used as a vector to project data onto. This process is repeated for each cluster of displacement data separated by a change in direction, and all 'best fit vector' projected data is combined for each GPS station to provide a continuous stream of representative horizontal displacement.

Determining the point at which magma movement progresses from one source to another was achieved through observing changes in the direction of displacement across all three GPS stations. This was easily identifiable for movement between the three sources identified in literature, with changes consistent across two or three GPS stations visible on the 5th March 2010 (Sill 1 to Sill 2) and the 17th March 2010 (Sill 2 to Dyke). However, the onset of Sill 1 inflation was harder to accurately identify. Seismicity began on the 6th January 2010, with deformation associated with sill inflation stated by Sigmundsson et al. (2010) to occur from December 2010.

Spatial plots of GPS movement from the IMO as an XY scatter graph (Figure 3) show clear changes in direction for all stations from the 4th March, correlating with an increase in seismic moment and number of earthquakes and suggesting a transition from proposed Sill 1 to Sill 2. Another change in direction for THEY is present from the 16th March, with an acceleration of movement in the same direction seen for SKOG, suggesting intrusion of the proposed Dyke. These changes are thought to reflect the varying locations of intrusions in relation to GPS stations, and are used to inform the 'best fit vectors' for projection of horizontal displacement data. STE2 data is considered less reliable, as gaps are present for Sill 1, Sill 2 appears to show a larger degree of noise, and less of a clear change in speed or direction is present for the Dyke.

Displacement data from all proposed sources were then projected onto their respective 'best fit vectors' and combined for each GPS station, in order to determine single streams of representative

daily horizontal ground movement from all stations that account for changes in source. This post-processed IMO data was considered a more effective proxy for stress than the radial displacement presented by Sigmundsson et al. (2010), and is hereafter referred to as 'horizontal displacement' to distinguish it.

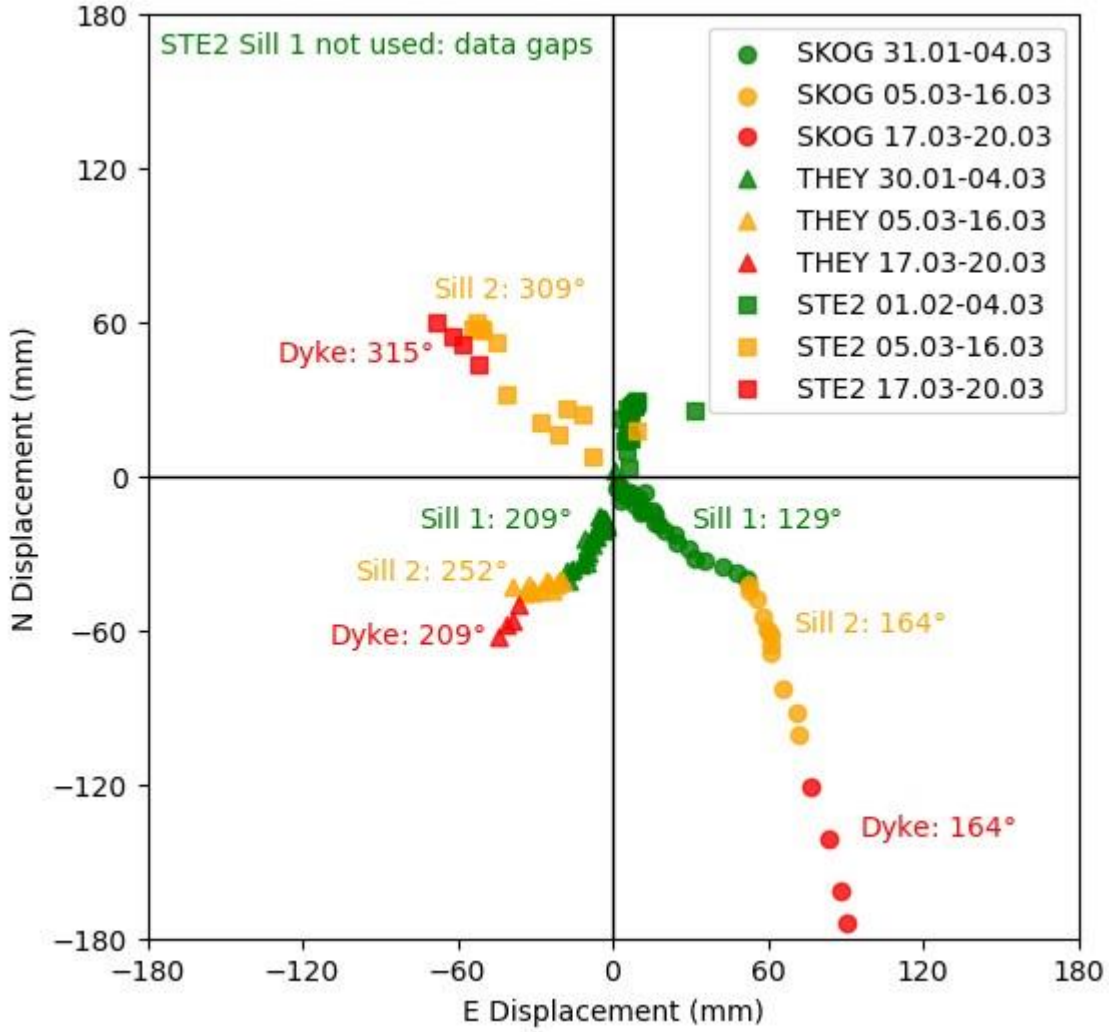

Figure 3: Plotted GPS horizontal displacements during the study period, coloured by proposed intrusion as shown in Figure 3.1a: 'Sill 1' (green), 'Sill 2' (orange) and 'Dyke' (red). Station 'SKOG' shown by dots, station 'THEY' shown by circles, and station 'STE2' shown by triangles.

3.2 Estimating source volume change from displacement:

In order to better analyse the relationship between seismicity and deformation during changes in the magma plumbing system, a time series of volume change across the study period would be required. As this data wasn't readily available, volume change was estimated using horizontal displacements and total source volume changes provided by InSAR data (Sigmundsson et al. 2010) by creating a constant of proportionality value (K) (Eq. 3).

$$K = V_t / D_t \tag{3}$$

Where V_t refers to the total volume change for a given time period (associated with the three proposed sources), and D_t is the total GPS horizontal displacement for that period. This equation was then used to create a time series of volume change (ΔV) using the daily horizontal displacement values (ΔD) (Eq. 4).

$$\Delta V = \Delta D \times K \tag{4}$$

Volume change estimation using this 'stable source' method assumes that recorded surface displacement is directly proportional to intruded volume change, and that this proportionality is constant for each GPS station across the growth of each source. This does not account for viscoelasticity, and would mean that the subsurface is completely elastic in nature. Given the relatively small changes in depth and horizontal extent between sources, variations in crustal strength were considered likely to be minimal. The basaltic composition of magma feeding the effusive flank eruption is also thought to be consistent and fed from a common deep source (unlike the later explosive summit eruption, which has evidence of magma mixing), based on petrological study of erupted material (Sigmundsson et al. 2010).

The stable source method also doesn't account for differences in source geometry, and assumes that the horizontal displacement is equally representative for all sources. For sill inflation it is usually the case that vertical displacement is greater, and therefore possible that using only horizontal displacement data may lose some finer detail and underestimate volume changes. However, GPS displacement data generally shows larger uncertainties for vertical movement than for horizontal, so any volume changes estimated will need to be checked to determine whether they are proportional to the total source volume change calculated from joint inversion of GPS and InSAR. Despite relying on these assumptions, source volume changes estimated using constants of proportionality were thought to be suitably accurate for comparison against seismic moment and analysis of the resulting relationship changes between sources. These volume change estimates were an equally efficient proxy for stress as horizontal displacement, as the two scale directly with one another, but also allowed for comparison with other studies.

3.3 Metrics to compare seismic and geodetic data

After digitising and examining seismicity and displacement monitoring data for notable characteristics, the datasets were compared against one another as a means of analysing their relationship. We calculated the ratio for cumulative seismic moment (ΣM_0) against source volume change estimated from post-processed IMO horizontal displacement using the stable source method (ΔV) for each GPS site, defined as αV (Eq. 5), in order to analyse changes across the entire study period as well as for each source individually. This ratio assumes a proportional relationship between horizontal displacement and volume change, due to the lack of directly obtainable time series volume change data.

$$\alpha V = \left| \frac{\Sigma M_0}{\Delta V} \right| \tag{5}$$

To better understand the processes behind changes in αV ratio, both between sources and within each source individually, we consider the effects of seismic efficiency (S_{EFF}) and shear modulus (G, introduced in Section 2.2). Eq. 6 shows that αV is equal to $\frac{\Sigma M_0}{\Delta V}$ from rearrangement of Eq. 2 as

presented in Clarke et al. (2019), and how increases to this ratio could be caused by either increasing S_{EFF} or shear modulus.

$$S_{EFF} = \frac{\Sigma M_0}{G\Delta V} \rightarrow \alpha V = \frac{\Sigma M_0}{\Delta V} = S_{EFF} \times G \quad (6)$$

Lab data from 276 uniaxial compression experiments performed on volcanic rocks, as presented within Heap et al. (2020), was used to estimate shear modulus for the proposed source depths in order to examine how seismic efficiency varies between sources.

3.4 Volume Estimate Results:

The time series of estimated volume change created using constants of proportionality (K), hereafter called the 'stable source method' (SSM), from horizontal displacement data and total source volume changes from joint inversion of GPS and InSAR (Sigmundsson et al. 2010) showed a good correlation between the two GPS stations, and an apparent exponential increase over the course of the study. This exponential trend was present for both the cumulative volume change over the entire study period (Figure 4a) and when each source volume change was plotted individually (Figure 4b). These trends within each source mirror those seen for horizontal displacement, but by relating these to source volume totals reported in Sigmundsson et al. (2010) this gives a representative time series of volume change.

The rate of change calculated for each source confirmed an exponential increase, with an average for both GPS stations of 4.1×10^5 m^3/day for Sill 1, 1.5×10^6 m^3/day for Sill 2, and 7.3×10^6 m^3/day for the Dyke. This increasing rate of change is due to a combination of the increased deformation during the development of Sill 2 and the Dyke, but also the shorter periods of time during which the latter two sources inflated.

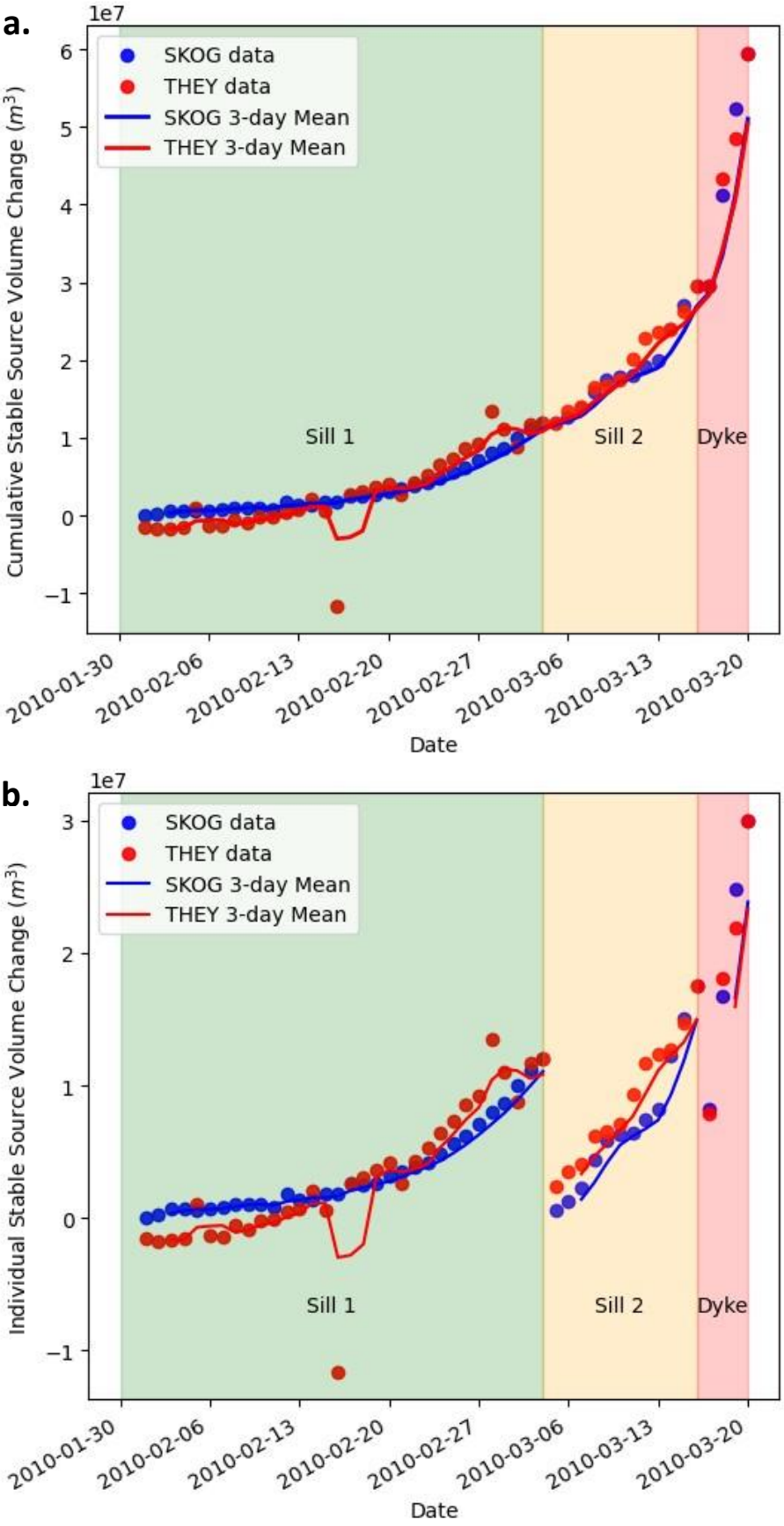

337 **Figure 4:** Estimated volume changes using the stable source method, based on horizontal displacement data,
338 with 3-day mean fitted. a. Cumulative volume change from all sources combined. b. Individual source volume
339 changes plotted separately.

3.4 Simplified ratios between seismic moment and volume change

Using the stable source method volume changes calculated, it was possible to create a time series plot of the ratio between seismic moment and volume change (αV), separated into the three proposed magmatic sources. Cumulative ratios (Figure 5a) for all sources showed an increase of 1.1×10^7 Nm/m^3 for both GPS stations THEY and SKOG from Sill 1 to Sill 2, and a decrease of 2.1×10^6 Nm/m^3 from Sill 2 to the Dyke. Individual source αV ratios (Figure 5b) show an increase of 1.5×10^8 Nm/m^3 (~2650%) from Sill 1 to Sill 2, and a decrease of 2.2×10^7 Nm/m^3 (~60%) from Sill 2 to the Dyke. A decrease in ratio is also seen within the latter two sources, with Sill 1 comparatively constant but with a degree of noise.

Unlike a ratio based purely on displacement data, where a change in surface deformation relating to sources at different depths was expected based on evidence presented in literature, the changes noted in αV between sources were not expected to occur. This is because it was thought that the rate of seismic moment release and volume change would remain proportional to one another, however despite the exponential volume increase shown in Figure 4 the onset of Sill 2 inflation saw a far greater increase in seismic moment.

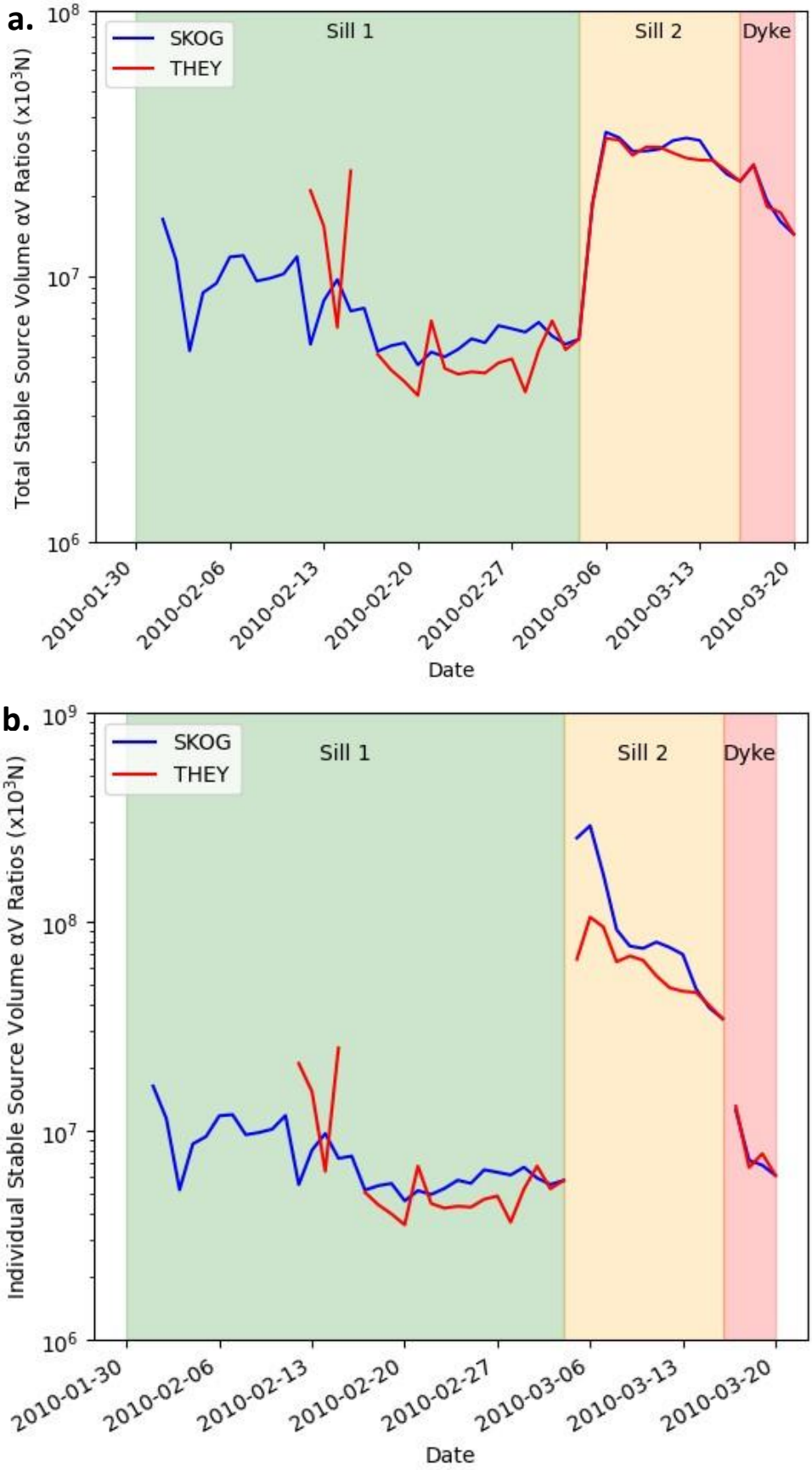

Figure 5: Plots of volume change ratios through time. **a.** αV ratio for all sources combined, using ΣM_0 and total volume change from all sources. **b.** Individual αV source ratios, calculated using individual seismic moments and stable source method volume changes.

4. Discussion:

4.1 Shear Modulus as a mechanism of volume change ratio

Upon plotting the ratio between moment and stable source volume change (αV), an increase from Sill 1 to Sill 2 was seen. It had been expected that the rate of seismic moment release and volume change would remain proportional to one another, resulting in a relatively consistent ratio across the study period. Therefore, further study was required to determine the processes responsible for the increase in αV between sources. As established in Section 3.3, changing αV is driven by shear modulus and seismic efficiency, so these are both examined individually.

Eq. 6 explains that αV ratio is comprised of seismic efficiency multiplied by shear modulus. Using the data and model presented by Heap et al. (2020) with a constant seismic efficiency of 1 and an assumed Poisson ratio of 0.25, a profile of shear modulus with depth was created (Figure 6). This revealed that shear modulus increases with depth, and therefore decreases with progression between sources. Heap et al.'s (2020) model gives values of ~15.4GPa for Sill 1 at a depth of 5500m, ~14.8GPa for Sill 2 at a depth of 4700m, and ~9.7GPa for the average Dyke depth; ~13.8GPa at the lower edge at a depth of 3800m, and ~5.6GPa at the upper edge at a depth of 100m. As the ratio between seismicity and ground deformation increases as magma moves from depth towards the surface, these changes do not correlate with one another and suggest that seismic efficiency, rather than shear modulus, is the cause of changing αV ratio.

Some examples suggest that shear modulus also increases with decreasing temperature for Icelandic basalts (Bakker et al. 2016, Lamur et al. 2018). Although the depth difference between sources is likely not large enough to cause significant cooling, the presence of intrusions from the 1990s (as discussed in Section 2.3) may have created a locally elevated geotherm that affects Sill 1. Estimated crystallisation temperatures for magma from the flank eruption were ~1170°C with a range of <30°C for any given depth (Keiding & Sigmarsson 2012), and for temperatures >900°C the effect on shear modulus appears to be negligible (Heap et al. 2020). There is a possibility that these temperatures may influence viscoelastic deformation of the crust and how surface deformation relates to volume change.

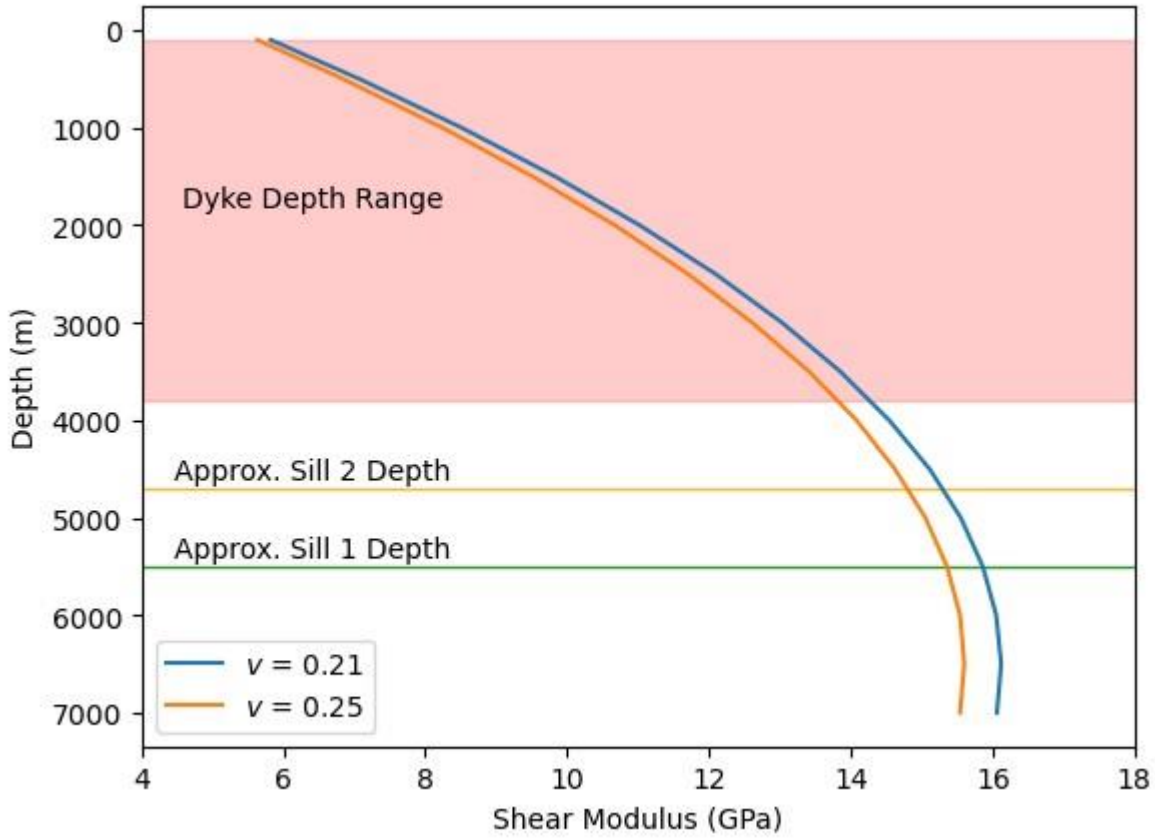

Figure 6: Changing Shear Modulus with depth, calculated based on information present within Heap et al. (2020) using varying Poisson ratios (v). Graph annotated with approximate depth of Sills and Dyke depth range according to Sigmundsson et al. (2010).

4.2 Seismic efficiency as a mechanism of volume change ratio

With an increase in seismic efficiency (S_{EFF}), more seismic moment is generated from earthquakes per unit of volume change. As shear modulus was found to increase with depth and therefore decrease during magma propagation between sources in our study, increased seismic efficiency with moment is the most likely cause of increased αV ratio from Sill 1 to Sill 2, and indicates a decrease in aseismic deformation between sources. Using cumulative seismic moment data, shear modulus for each source depth as determined from Heap et al. (2020), and total volume change from horizontal displacement using the stable source method, a plot of seismic efficiency through time (Figure 7) shows an increase for Sill 2 compared to Sill 1 similar to that seen for αV ratio. A similar increase in seismic efficiency is also present at the onset of Dyke propagation, which is not seen in αV but does correspond to a spike in seismic moment.

One possible reason for changes in seismic efficiency is subsurface heterogeneity in crustal stress and strength, with Sill 1 building pressure from deep magmatic injection in a higher temperature, low-density layer of host rock until sufficient for the intrusion to ascend to shallower depths (Sigmundsson et al. 2010). Movement of magma through colder, more brittle crust then causes more stress to be released seismically, resulting in an increased rate of change for strain and higher seismic efficiency. However, as crustal strength changes with depth were examined in Section 4.1 through shear modulus, this was determined not to be responsible.

Instead, the increase and variations present within Sill 2 for the two GPS stations examined (THEY and SKOG, given their completeness for all three sources compared to STE2) may relate to the periodic

activation of seismogenic faults separating a number of 'lobes' of magma within the sill (Tarasewicz et al. 2014). As pressure increases with injection of new magma these faults rupture, causing increased seismicity. These variations in seismic efficiency occur when there is a spike in daily seismic moment compared to cumulative volume change (which appears to increase at a relatively stable rate throughout the growth of Sill 2, as shown in Figure 4), and is thought to illustrate the change from aseismic lobe growth, with stress change accommodated by the elasticity of the crust, to the opening of faults between the lobes once a threshold or yield stress is reached.

Evidence of lobed inflation can be seen within the horizontal displacement data, as a spike is seen in the SKOG GPS station on the 14th March that is not reflected in the THEY station (suggesting non-uniform sill growth). Daily seismic moment release also became negligible on the 14th following elevated values in the preceding days, indicating a time lag between the rupturing of faults and intrusion of magma. Intrusion of the Dyke was also thought to cause fracturing of the surrounding country rock, causing a period of increased seismicity in the 4 days prior to eruption, however as this was accompanied by increased displacement the overall αV ratio is seen to decrease slightly.

The similarity between Figures 4a and 6 confirms that changing seismic efficiency is the main driver of αV ratio for Sill 2. Changing shear modulus with depth has greater influence over Dyke αV ratio, with seismic efficiency appearing much lower if shear modulus is the same as for Sill 2 (mirroring Figure 4a).

Previous studies examining total seismic moment and volume change data, such as McGarr (2014) and Meyer et al. (2021), give an array of seismic efficiency values that differ by several orders of magnitude depending on both seismic moment and total volume change. Although not presented within literature, seismic efficiencies can be calculated for these studies using available seismic moment, volume change, and shear moduli values. Hallo et al. (2014) states that typical ranges for seismic efficiency are between 10^{-2} and 1.0 for enhanced geothermal systems, and 5×10^{-7} and 5×10^{-4} for hydraulic fracturing of rocks, although does also state that the variability and modelling of seismic efficiency are poorly understood. This uncertainty is highlighted by the fact that some case studies presented in Hallo et al. (2014) show seismic efficiencies of up to 2.3. The seismic efficiencies calculated for our case study range from 2.3×10^{-4} to 1.6×10^{-3} for Sill 1, 10^{-3} to 2.3×10^{-3} for Sill 2, and 1.5×10^{-3} to 2.1×10^{-3} for the Dyke. These values are higher than those given by Hallo et al. (2014) for fracturing of rocks, but are within an order of magnitude and so considered sensible given the uncertainties noted.

Well injection data presented by McGarr (2014) generally yields much higher seismic efficiencies than our study (between 5.2×10^{-2} and 2.6), for a similar shear modulus (14.7GPa) and seismic moment values (3.2×10^{12} to 8.9×10^{14} Nm). This discrepancy is likely due to the different scenarios associated with the two datasets, as McGarr's (2014) well injection case studies agree with Hallo et al.'s (2014) range for geothermal systems, whereas our volcanic unrest data is closer to the range for hydraulic fracturing of rock. The injected volumes for McGarr's (2014) data are 2 to 3 orders of magnitude lower than our data for a similar seismic moment, likely due to less aseismic deformation within the host rock. This is reflected in another description of the two ranges for seismic efficiency within Hallo et al. (2014), with typical values for geothermal and hydraulic fracturing also referred to as for 'hard rock' and 'soft rock' respectively.

Meyer et al.'s (2021) case studies for volcanic unrest yield a wide range of seismic efficiencies (2.3×10^{-10} to 1.1) using the same shear modulus of 14.7GPa as for McGarr (2014), due to the range of volcanic scenarios, cumulative seismic moments and intruded volume changes present. Data for the 2010 unrest episode at Eyjafjallajökull yields a seismic efficiency value far closer to those presented in Figure

6.2 (1.3×10^{-3}) than other events within Meyer et al.'s (2021) dataset. Changing the shear modulus for Meyer et al.'s (2021) case studies within the range calculated using Heap et al. (2020) data for depths up to 7km (as shown in Figure 5) makes little difference to the seismic efficiency, generally within an order of magnitude. This further confirms that shear modulus is likely to play a minimal role in the relationship between seismic moment and volume change, without significant changes in depth or host rock strength.

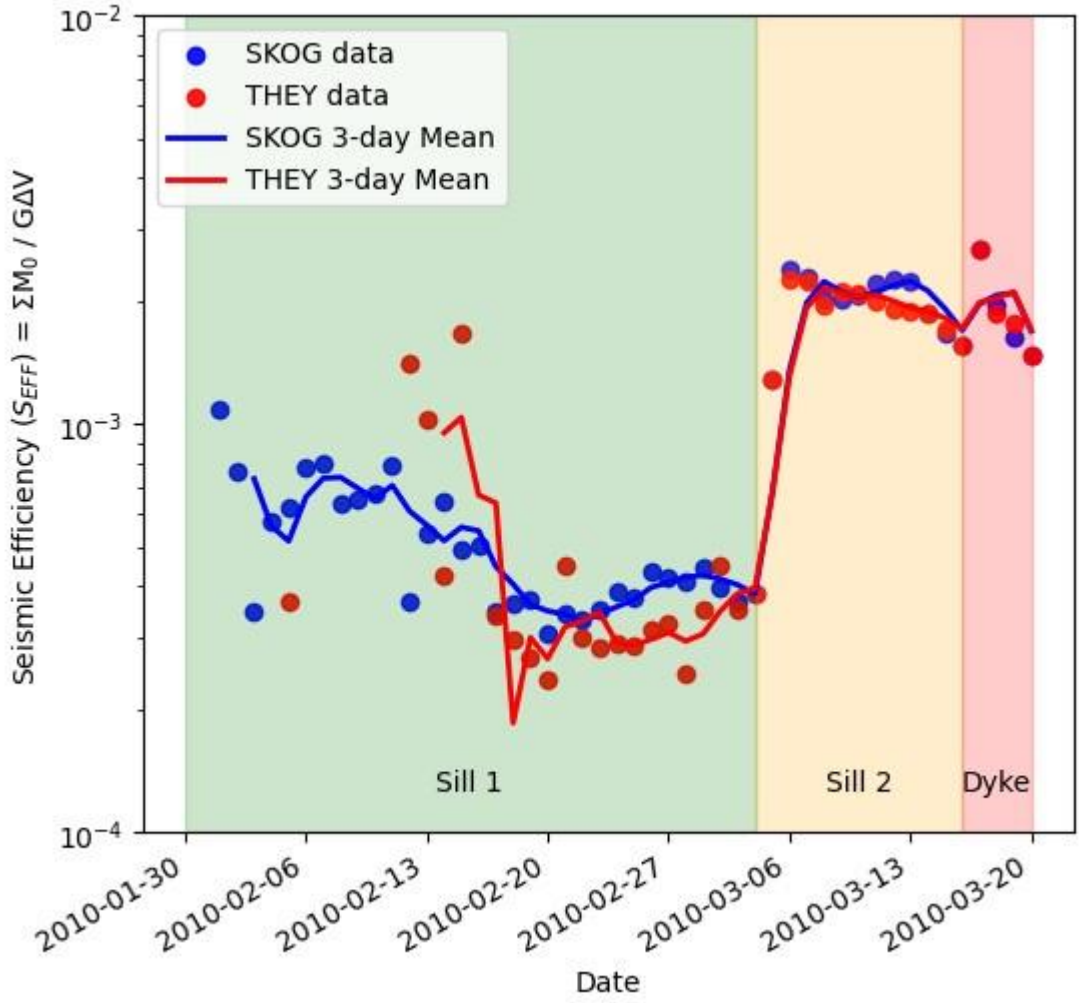

Figure 7: Time series plot of seismic efficiency, derived using cumulative seismic moment, total volume change estimated from constants of proportionality (K) and shear moduli for sources at varying depths as derived from Heap et al. (2020).

5. Conclusions:

5.1 Assumptions and Uncertainties:

Using seismic moment and GPS displacement data, we were able to identify the timing of magma movement between three sources identified in literature, apply post processing to show representative daily horizontal displacement through the use of best fit vectors, and compare the two parameters against one another to perform a basic analysis of how their relationship changes through time. We were then able to estimate volume change through time from displacement, using source

parameters from joint inversion of GPS and InSAR, and use this time series volume change data to perform more detailed analysis of the relationship between stress and strain.

Source parameters were also used alongside information in literature to determine how shear modulus changed with source depth, and establish that seismic efficiency was driving changes in ratio between seismic moment and estimated source volume change. Although the monitoring data used for our case study was comprehensive and the eruption well-studied, a number of assumptions had to be made about the available data, source parameters and the implementation of modelling techniques. Assumptions were also made regarding past studies in literature, in order to effectively compare these against our case study to find parallels and differences that could aid in volcanic eruption forecasting.

Use of the stable source method required assumptions to be made about horizontal displacement being directly proportional to source volume change, not accounting for GPS station location, errors in the data, and discounting vertical displacement. This method also doesn't directly account for non-uniform source growth and changes in source parameters such as depth, however volume change estimates are based on total source volume change values modelled through joint inversion of GPS and InSAR which does account for these parameters.

5.2 Scope for Future Work:

Our study has proved that in-depth analysis of volcano monitoring data and comparison of proxies for stress and strain against one another can produce new insights into the development of magma plumbing systems prior to eruptive activity, and highlight similarities and differences with relationships between stress and strain seen in literature. But in order to better understand how the relationship between seismic moment and intruded source volume change may differ for unrest episodes around the world, and how this could be used to aid in forecasting of eruptive activity over month to year timescales, similar study of past unrest episodes is required.

We believe that in addition to further study of total seismic moment and intruded volume change for a greater number of unrest episodes, examining time series relationships of source growth within these events will allow for further insight into what characteristics may be responsible for similarities between inflating sources. It may also be possible with more comprehensive datasets over a range of volcanic scenarios to identify whether certain volcanic settings show characteristic changes in relationship immediately prior to eruption. This behaviour was not identified during our case study, likely due to either the effusive nature of the eruption or the short growth period of the Dyke feeding the eruption. If multiple past unrest episodes sharing eruption types or other characteristics show similar relationships between moment and volume leading to eruption, this could then be used as a forecasting tool for better constraining the timing of volcanic activity onset.

Other volcanoes that could provide high quality time series monitoring data to compare to our study of Eyjafjallajökull would preferably have experienced unrest within the last decade, as well as multiple previous episodes of unrest not all resulting in eruption. This combination of historic and recent activity is likely to mean a comprehensive monitoring network is in place for all of the most recent episode, and past data from a variety of unrest episodes will allow for comparison within a single tectonic setting similar to that conducted for our multiple sources. Some examples of potential candidate volcanoes for further study could include El Hierro and La Palma in the Canary Islands, where the 2011 and 2021 eruptions could be compared against one another given their similar tectonic setting and geographical location, and Hawaii, which has undergone multiple periods of unrest in recent history and is well-studied.

Another volcano which shows potential for time series analysis of unrest surrounding multiple eruptions is Sierra Negra, as demonstrated within Bell et al. (2021). This study shows the relationship between seismic moment and uplift between eruptions in 2005 and 2018, and appears to show an overall relationship similar to our case study. This observation would require further investigation, as currently displacement is only shown in one direction (vertical uplift). Based on the data available for our case study, horizontal displacement may show lower uncertainty. The tectonic setting of Sierra Negra is also fairly unique, as seismicity occurs along established 'trap-door' faults around the volcano caldera. Such observations linking volcano characteristics and different relationships are likely to be invaluable to forecasting efforts.

6. References

Albino, F., J. Biggs and D. K. Syahbana (2019). "Dyke intrusion between neighbouring arc volcanoes responsible for 2017 pre-eruptive seismic swarm at Agung." Nat Commun **10**(1): 748.

Albino, F., Biggs, J., Lazecký, M. and Maghsoudi, Y. (2022). "Routine processing and automatic detection of volcanic ground deformation using Sentinel-1 InSAR data: insights from African volcanoes." Remote Sensing, **14**(22), p.5703.

Bakker, R. R., M. Frehner and M. Lupi (2016). "How temperature-dependent elasticity alters host rock/magmatic reservoir models: A case study on the effects of ice-cap unloading on shallow volcanic systems." Earth and Planetary Science Letters **456**: 16-25.

Battaglia, M., J. Gottsmann, D. Carbone and J. Fernández (2008). "4D volcano gravimetry." Geophysics **73**(6): WA3-WA18.

Bell, A. F., J. Greenhough, M. J. Heap and I. G. Main (2011). "Challenges for forecasting based on accelerating rates of earthquakes at volcanoes and laboratory analogues." Geophysical Journal International **185**(2): 718-723.

Bell, A. F., S. Hernandez, P. C. La Femina and M. C. Ruiz (2021). "Uplift and Seismicity Driven by Magmatic Inflation at Sierra Negra Volcano, Galápagos Islands." Journal of Geophysical Research: Solid Earth **126**(7): e2021JB022244.

Bell, A. F., M. Naylor and I. G. Main (2013). "The limits of predictability of volcanic eruptions from accelerating rates of earthquakes." Geophysical Journal International **194**(3): 1541-1553.

Biggs, J., Bastow, I.D., Keir, D. and Lewi, E. (2011). "Pulses of deformation reveal frequently recurring shallow magmatic activity beneath the Main Ethiopian Rift." Geochemistry, Geophysics, Geosystems, **12**(9).

Biggs, J. and M. E. Pritchard (2017). "Global Volcano Monitoring: What Does It Mean When Volcanoes Deform?" Elements **13**(1): 17-22.

Burton, M. R., G. G. Salerno, L. D'Auria, T. Caltabiano, F. Murè and R. Maugeri (2015). "SO 2 flux monitoring at Stromboli with the new permanent INGV SO 2 camera system: A comparison with the FLAME network and seismological data." Journal of Volcanology and Geothermal Research **300**: 95-102.

Caricchi, L., J. Biggs, C. Annen and S. Ebmeier (2014). "The influence of cooling, crystallisation and re-melting on the interpretation of geodetic signals in volcanic systems." Earth and Planetary Science Letters **388**: 166-174.

Chaussard, E. and Amelung, F. (2012). “Precursory inflation of shallow magma reservoirs at west Sunda volcanoes detected by InSAR.” Geophysical Research Letters, **39**(21).

Clarke, H., J. P. Verdon, T. Kettlety, A. F. Baird and J. M. Kendall (2019). "Real-Time Imaging, Forecasting, and Management of Human-Induced Seismicity at Preston New Road, Lancashire, England." Seismological Research Letters **90**(5): 1902-1915.

Cornelius, R. R. and B. Voight (1995). "Graphical and PC-software analysis of volcano eruption precursors according to the Materials Failure Forecast Method (FFM)." Journal of Volcanology and Geothermal Research **64**(3-4): 295-320.

Fialko, Y., Y. Khazan and M. Simons (2001). "Deformation due to a pressurized horizontal circular crack in an elastic half-space, with applications to volcano geodesy." Geophysical Journal International **146**(1): 181-190.

Hallo, M., I. Oprsal, L. Eisner and M. Y. Ali (2014). "Prediction of magnitude of the largest potentially induced seismic event." Journal of Seismology **18**(3): 421-431.

Heap, M. J., M. Villeneuve, F. Albino, J. I. Farquharson, E. Brothelande, F. Amelung, J.-L. Got and P. Baud (2020). "Towards more realistic values of elastic moduli for volcano modelling." Journal of Volcanology and Geothermal Research **390**: 106684.

Hjaltadóttir, S., K. S. Vogfjörð and R. Slunga (2009). "Seismic signs of magma pathways through the crust in the Eyjafjallajökull volcano, South Iceland." Report, VÍ/2009 **13**: 33.

Hreinsdottir, S., F. Sigmundsson, M. Roberts, P. Árnadóttir, B. Ófeigsson, R. Grapenthin, E. Sturkell, T. Villemin, R. Bennett and H. Geirsson (2012). The 2010 Eyjafjallajökull and 2011 Grímsvötn eruptions: Insights from GPS geodesy**:** 13577.

Illsley-Kemp, F., S. J. Barker, C. J. N. Wilson, C. J. Chamberlain, S. Hreinsdóttir, S. Ellis, I. J. Hamling, M. K. Savage, E. R. H. Mestel and F. B. Wadsworth (2021). "Volcanic Unrest at Taupō Volcano in 2019: Causes, Mechanisms and Implications." Geochemistry, Geophysics, Geosystems **22**(6): e2021GC009803.

Johnson, J. H. and M. P. Poland (2013). "Seismic detection of increased degassing before Kilauea's 2008 summit explosion." Nat Commun **4**: 1668.

Keiding, J. K. and O. Sigmarsson (2012). "Geothermobarometry of the 2010 Eyjafjallajökull eruption: New constraints on Icelandic magma plumbing systems." Journal of Geophysical Research: Solid Earth **117**(B9), doi:10.1029/2011JB008829.

Kilbride, B. M., M. Edmonds and J. Biggs (2016). "Observing eruptions of gas-rich compressible magmas from space." Nat Commun **7**: 13744.

Kilburn, C. (2012). "Precursory deformation and fracture before brittle rock failure and potential application to volcanic unrest." Journal of Geophysical Research: Solid Earth **117**(B2), doi:10.1029/2011JB008703.

Lamur, A., Y. Lavallee, F. E. Iddon, A. J. Hornby, J. E. Kendrick, F. W. von Aulock and F. B. Wadsworth (2018). "Disclosing the temperature of columnar jointing in lavas." Nat Commun **9**(1): 1432.

Le Mével, H., K. L. Feigl, L. Córdova, C. DeMets and P. Lundgren (2015). "Evolution of unrest at Laguna del Maule volcanic field (Chile) from InSAR and GPS measurements, 2003 to 2014." Geophysical Research Letters **42**(16): 6590-6598.

López, C., M. A. Benito-Saz, J. Martí, C. del-Fresno, L. García-Cañada, H. Albert and H. Lamolda (2017). "Driving magma to the surface: The 2011–2012 El Hierro Volcanic Eruption." Geochemistry, Geophysics, Geosystems **18**(8): 3165-3184.

McGarr, A. (2014). "Maximum magnitude earthquakes induced by fluid injection." Journal of Geophysical Research: Solid Earth **119**(2): 1008-1019.

Meyer, K., J. Biggs and W. Aspinall (2021). "A Bayesian reassessment of the relationship between seismic moment and magmatic intrusion volume during volcanic unrest." Journal of Volcanology and Geothermal Research **419**: 107375.

Miensopust, M. P., A. G. Jones, G. P. Hersir and A. M. Vilhjálmsson (2014). "The Eyjafjallajökull volcanic system, Iceland: insights from electromagnetic measurements." Geophysical Journal International **199**(2): 1187-1204.

Okada, Y. (1985). "Surface deformation due to shear and tensile faults in a half-space." Bulletin of the seismological society of America **75**(4): 1135-1154.

Pedersen, R. and F. Sigmundsson (2004). "InSAR based sill model links spatially offset areas of deformation and seismicity for the 1994 unrest episode at Eyjafjallajökull volcano, Iceland." Geophysical Research Letters **31**(14), doi:10.1029/2004GL020368.

Pedersen, R. and F. Sigmundsson (2006). "Temporal development of the 1999 intrusive episode in the Eyjafjallajökull volcano, Iceland, derived from InSAR images." Bulletin of Volcanology **68**(4): 377-393.

Pritchard, M. E., T. A. Mather, S. R. McNutt, F. J. Delgado and K. Reath (2019). "Thoughts on the criteria to determine the origin of volcanic unrest as magmatic or non-magmatic." Philos Trans A Math Phys Eng Sci **377**(2139): 20180008.

Reath, K., M. Pritchard, J. Biggs, B. Andrews, S. K. Ebmeier, M. Bagnardi, T. Girona, P. Lundgren, T. Lopez and M. Poland (2020). "Using Conceptual Models to Relate Multiparameter Satellite Data to Subsurface Volcanic Processes in Latin America." Geochemistry, Geophysics, Geosystems **21**(1): e2019GC008494.

Reddin, E., Ebmeier, S.K., Rivalta, E., Bagnardi, M., Baker, S., Bell, A.F., Mothes, P. and Aguaiza, S. (2023). “Magmatic connectivity among six Galápagos volcanoes revealed by satellite geodesy.” Nature Communications, **14**(1), p.6614.

Rodgers, M., P. J. Smith, T. A. Mather and D. M. Pyle (2016). "Quiescent-explosive transitions during dome-forming volcanic eruptions: Using seismicity to probe the volcanic processes leading to the 29 July 2008 vulcanian explosion of Soufrière Hills Volcano, Montserrat." Journal of Geophysical Research: Solid Earth **121**(12): 8453-8471.

Sandri, L., W. Marzocchi and L. Zaccarelli (2004). "A new perspective in identifying the precursory patterns of eruptions." Bulletin of Volcanology **66**(3): 263-275.

Schmid, A., J. R. Grasso, D. Clarke, V. Ferrazzini, P. Bachèlery and T. Staudacher (2012). "Eruption forerunners from multiparameter monitoring and application for eruptions time predictability

(Piton de la Fournaise)." Journal of Geophysical Research: Solid Earth **117**(B11), doi:10.1029/2012JB009167.

Scholz, C. H. (1968). "Microfracturing and the inelastic deformation of rock in compression." Journal of Geophysical Research **73**(4): 1417-1432.

Segall, P., A. L. Llenos, S. H. Yun, A. M. Bradley and E. M. Syracuse (2013). "Time-dependent dike propagation from joint inversion of seismicity and deformation data." Journal of Geophysical Research: Solid Earth **118**(11): 5785-5804.

Sheldrake, T. E., W. P. Aspinall, H. M. Odbert, G. Wadge and R. S. J. Sparks (2017). "Understanding causality and uncertainty in volcanic observations: An example of forecasting eruptive activity on Soufrière Hills Volcano, Montserrat." Journal of Volcanology and Geothermal Research **341**: 287-300.

Sigmundsson, F., S. Hreinsdottir, A. Hooper, T. Arnadottir, R. Pedersen, M. J. Roberts, N. Oskarsson, A. Auriac, J. Decriem, P. Einarsson, H. Geirsson, M. Hensch, B. G. Ofeigsson, E. Sturkell, H. Sveinbjornsson and K. L. Feigl (2010). "Intrusion triggering of the 2010 Eyjafjallajokull explosive eruption." Nature **468**(7322): 426-430.

Sparks, R. S. J. (2003). "Forecasting volcanic eruptions." Earth and Planetary Science Letters **210**(1-2): 1-15.

Sparks, R. S. J., J. Biggs and J. Neuberg (2012). "Monitoring volcanoes." Science **335**(6074): 1310-1311.

Syahbana, D. K., K. Kasbani, G. Suantika, O. Prambada, A. S. Andreas, U. B. Saing, S. L. Kunrat, S. Andreastuti, M. Martanto, E. Kriswati, Y. Suparman, H. Humaida, S. Ogburn, P. J. Kelly, J. Wellik, H. M. N. Wright, J. D. Pesicek, R. Wessels, C. Kern, M. Lisowski, A. Diefenbach, M. Poland, F. Beauducel, J. Pallister, R. G. Vaughan and J. B. Lowenstern (2019). "The 2017-19 activity at Mount Agung in Bali (Indonesia): Intense unrest, monitoring, crisis response, evacuation, and eruption." Sci Rep **9**(1): 8848.

Tarasewicz, J., B. Brandsdóttir, R. S. White, M. Hensch and B. Thorbjarnardóttir (2012). "Using microearthquakes to track repeated magma intrusions beneath the Eyjafjallajökull stratovolcano, Iceland." Journal of Geophysical Research: Solid Earth **117**(B9), doi:10.1029/2011JB008751.

Tarasewicz, J., White, R. S., Woods, A. W., Brandsdóttir, B., & Gudmundsson, M. T. (2012). “Magma mobilization by downward-propagating decompression of the Eyjafjallajökull volcanic plumbing system.” Geophysical Research Letters, **39**(19).

Tarasewicz, J., R. S. White, B. Brandsdóttir and C. M. Schoonman (2014). "Seismogenic magma intrusion before the 2010 eruption of Eyjafjallajökull volcano, Iceland." Geophysical Journal International **198**(2): 906-921.

Verdon, J.P., Pullen, B. and Rodríguez-Pradilla, G. (2024). “Growth and stabilization of induced seismicity rates during long-term, low-pressure fluid injection.” Philosophical Transactions A, **382**(2276), p.20230183.

Vila, J., R. Ortiz, M. Tárraga, R. Macià, A. García, D. Kumar and A. Correig (2008). "Near-Real time analysis of seismic data of active volcanoes: Software implementations of time sequence data analysis." Natural Hazards and Earth System Sciences **8**(4): 789-794.

672 Wellik, J. J., S. G. Prejean and D. K. Syahbana (2021). "Repeating Earthquakes During Multiple Phases
673 of Unrest and Eruption at Mount Agung, Bali, Indonesia, 2017." Frontiers in Earth Science **9**:
674 653164.

675 Werner, C., J. A. Power, P. J. Kelly, S. Prejean and C. Kern (2022). "Characterizing unrest: A
676 retrospective look at 20 years of gas emissions and seismicity at Iliamna Volcano, Alaska." Journal
677 of Volcanology and Geothermal Research **422**: 107448.

678 White, R. and W. McCausland (2016). "Volcano-tectonic earthquakes: A new tool for estimating
679 intrusive volumes and forecasting eruptions." Journal of Volcanology and Geothermal Research
680 **309**: 139-155.